

# Silicon/Graphite/Polyaniline Nanocomposite with Improved Lithium-Storage Capacity and Cyclability as Anode Materials for Lithium-ion Batteries

Meng Chen<sup>1</sup>, Chunyu Du<sup>2,\*</sup>, Long Wang<sup>1</sup>, Geping Yin<sup>2</sup>, Pengfei Shi<sup>2</sup>

<sup>1</sup> School of Chemistry and Materials Science, Harbin Engineering University, Harbin 150080, China

<sup>2</sup> School of Chemical Engineering & Technology, Harbin Institute of Technology, Harbin 150001, China

\*E-mail: [cydu@hit.edu.cn](mailto:cydu@hit.edu.cn)

Received: 10 October 2011 / Accepted: 25 November 2011 / Published: 1 January 2012

---

A silicon/graphite/polyaniline (Si/G/PANI) nanocomposite is facilely prepared by the in-situ chemical polymerization of aniline monomer in the presence of nano-Si and graphite powders. This composite are examined by scanning electronic microscopy, transmission electronic microscopy, Raman spectroscopy, Fourier-transform infrared spectroscopy, and electrochemical measurements. It is observed that the composite consists of nanosized silicon and graphite distributed uniformly in a polyaniline matrix. Galvanostatic charge-discharge profiles and cycling curves reveal that the Si/G/PANI composite exhibits good electrochemical performance: a high reversible specific capacity of 1392 mAh g<sup>-1</sup> for the first cycle and a stable capacity retention with 866 mAh g<sup>-1</sup> after 95 cycles. In contrast, pure Si nanoparticles only deliver the reversible capacity of 888 mAh g<sup>-1</sup> and 425 mAh g<sup>-1</sup> for the first and the 95<sup>th</sup> cycles, respectively. The enhanced electrochemical performance is mainly attributed to the reinforced electric contact of active materials, better dispersion of Si nanoparticles, and good structural stability of the Si/G/PANI composite electrode during the charge-discharge process, which originate largely from the presence of PANI.

---

**Keywords:** lithium-ion batteries, anode, silicon/graphite/polyaniline composite, specific capacity, cyclability

## 1. INTRODUCTION

At present, graphite has commonly been used as the anode material for lithium-ion batteries (LIBs), because of its low and flat working potential, high coulombic efficiency, good cyclability, etc [1]. However, the theoretical capacity of graphite is only 370 mAh g<sup>-1</sup>, significantly limiting the

specific energy of LIBs [2]. Thus, to meet the increasing demand for high energy density LIBs, alternative anode materials with higher capacity are in urgent need. Among various candidates, silicon (Si) stands out due to its extremely high capacity with the maximum Li uptake of  $\text{Li}_{4.4}\text{Si}$ , corresponding to  $4200 \text{ mAh g}^{-1}$  of theoretical capacity [3]. Unfortunately, it is well known that a big volume change ( $>300\%$ ) is associated with the lithium intercalation and extraction process of Si. This change causes great stress in Si lattice and thus leads to cracking and crumbling of Si particles. As a result, reversible capacity of Si fades abruptly only after several cycles of charge and discharge [4,5].

In the last decade, many research efforts have been carried out to mitigate the severe volume change of Si [6,7]. The most common and facile approach is to disperse Si particles within an active or inactive solid host matrix [8-10]. The host matrix acts as a buffer to accommodate the severe volume change of Si, thereby preventing its pulverization and crumbling.

Apparently, the matrix must have a good mechanical property to withstand the severe volume change of Si during cycling. Also, it should have high electronic conductivity to allow charge transfer reactions to take place. Carbon is usually utilized as the host matrix, because it not only is highly conductive, but also contributes to the capacity since Li can be intercalated into carbon as well [11-13]. It is widely reported that Si/C composites show better cycling stability than bare Si [14]. Nevertheless, the capacity retention is still not satisfactory for practical applications, indicating that the carbon matrix alone is not able to completely constrain the severe volume change of Si [15]. In addition, high temperature pyrolysis is often utilized for the preparation of Si/C composites, which is high energy consuming and not environment-friendly.

Conductive polymers have been used in various energy conversion and storage applications such as fuel cells and supercapacitors, because they combine flexibility, toughness, malleability and elasticity of polymers with high electrical conductivity [16-18]. It can be imagined that if a conductive polymer is used as the host matrix for Si anode materials, some distinguished advantages can thus be obtained: (1) the soft conductive polymer matrix can efficiently buffer the severe volume changes of Si during the  $\text{Li}^+$  intercalation and extraction process, hence improving cyclability of the Si anode; (2) the polymers act as a conductive binder, decreasing the contact resistance between Si particles; (3) the conductive polymers also facilitate the dispersion of Si particles, especially Si nanoparticles, leading to larger Si/electrolyte interface and therefore improved reversible capacity.

As a unique conductive polymer, polyaniline (PANI) has attracted much attention due to its ease of synthesis, environmental stability, and simple doping/dedoping chemistry. However, as far as we know, there have been no reports to date on the use of PANI as a host matrix for the Si anode material. The goal of present study is to explore the possibility of PANI as a host matrix for the nano-Si anode material.

Meanwhile, in order to improve performance of the Si material, small amount of graphite is also added to obtain a Si/graphite/polyaniline (Si/G/PANI) nanocomposite. The Si/G/PANI composite was prepared by an in-situ chemical polymerization method, and characterized by scanning electronic microscopy (SEM), transmission electronic microscopy (TEM), Raman spectroscopy and Fourier-transform infrared (FTIR) spectroscopy.

Electrochemical performance of the Si/G/PANI composite was evaluated by charge-discharge profiles, electrochemical impedance spectroscopy (EIS), and cycling capacity curves. It was found that

the Si/G/PANI composite showed greatly improved lithium-storage performance and good cycling stability.

## 2. EXPERIMENTAL

The Si/G/PANI composite was prepared by an in-situ chemical polymerization method with HCl as the dopant and  $(\text{NH}_4)_2\text{S}_2\text{O}_8$  as the oxidant. Briefly, 1.82 mL aniline monomer was first mixed with 150 ml of 0.1 M HCl solution by continuous stirring. Then crystalline Si nanopowder (size: 80-100 nm, 99%, Kaier Nanometer, China) and artificial graphite (averaged size: 21  $\mu\text{m}$ , 99%, BTR, China) were added into the mixture via ultrasonication for 30 min. Afterwards, 0.5 M  $(\text{NH}_4)_2\text{S}_2\text{O}_8$  solution was slowly added under vigorous stirring. The reaction mixture was subsequently kept under stirring for 6 h in an ice-water bath. The greenblack reaction precipitate was filtered, and washed thoroughly with deionized water until free of  $\text{SO}_4^{2-}$ . Finally, the precipitate was dried in vacuum at 60  $^\circ\text{C}$  and then grinded to obtain the Si/G/PANI composite. The molar ratio of aniline monomer:HCl: $(\text{NH}_4)_2\text{S}_2\text{O}_8$  was 1:1:1, and the weight ratio of aniline monomer, graphite, and Si powder was 35:5:60. For comparison, the graphite/polyaniline (G/PANI) composite was also prepared by the same procedure except that no Si nanopowder was added.

SEM and TEM were performed using a JEM 100CX-II scanning electronic microscope and a Hitachi-7650 transmission electronic microscope, respectively. Raman spectroscopy characterization was carried out using a JOBIN YVON HR800 Confocal Raman system. FTIR spectroscopy was obtained using a PE Spectrum One FTIR spectrometer.

The electrochemical tests were performed using coin cells. The Si/G/PANI, pure Si, and G/PANI electrodes were prepared by dispersing 80% active materials, 10% acetylene carbon black and 10% carboxyl methyl cellulose (CMC) binder in the citric acid solution (pH=1.8) to form a homogeneous slurry. The slurry was then coated on a copper foil. After drying at 60  $^\circ\text{C}$  in a vacuum oven for 24 h, the copper foil with the above active materials were punched into circular discs with a diameter of 1.4 cm and then pressed at a pressure of 10 MPa to use as the working electrodes. Coin cells were assembled in an argon filled glove box, where the counter electrode was Li metal and the electrolyte was 1 M  $\text{LiPF}_6$  in a mixture of ethylene carbonate (EC), ethyl methyl carbonate (EMC) and dimethyl carbonate (DEC) (1:1:1, in volume). The cells were galvanostatically charged and discharged at 100 mA  $\text{g}^{-1}$  over the voltage range of 0.02~1.5 V (vs.  $\text{Li}^+/\text{Li}$ ) at room temperature. EIS measurements were carried out in a frequency range of 0.01 Hz and 100 kHz with an amplitude of 5 mV.

## 3. RESULTS AND DISCUSSION

### 3.1. Physical characterization

Morphology of pure Si and the Si/G/PANI composite was characterized by TEM and the results are shown in Fig. 1A and B. In Fig. 1A, most of the pure Si nanoparticles (NPs) were

spheroidal or ellipsoidal with size ranged from 40 to 150 nm, although some irregular ones were also observed. In addition, the surfaces of Si NPs was smooth, implying that the Si NPs were crystalline. For the Si/G/PANI composite (Fig. 1B), however, the Si surfaces became rough and a large amount of amorphous films or particles with thickness or size of <math><40\text{ nm}</math> (indicated by arrows) were observed, indicating the formation of PANI because the content of graphite was small and the size of graphite was generally in the range of >math>10\text{ }\mu\text{m}</math>. The presence of PANI tightly bound Si NPs together, which was beneficial to the electronic contact of Si NPs.

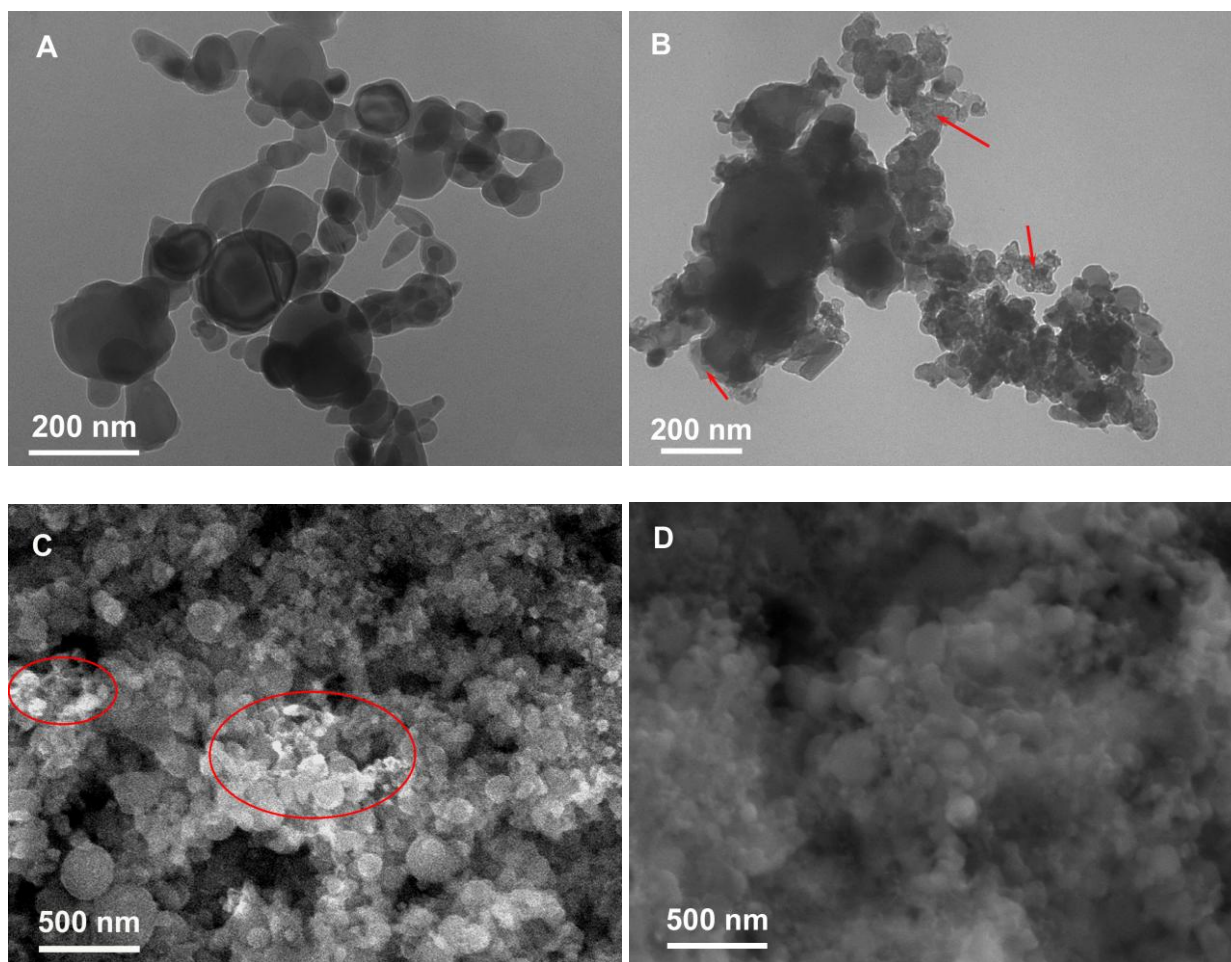


**Figure 1.** TEM images of pure Si nanoparticles (A) and the Si/G/PANI composite (B), and SEM images of the pure Si (C) and the Si/G/PANI composite (D) electrodes.

Fig. 1C and D present SEM images of the pure Si and Si/G/PANI composite electrodes, respectively. For the pure Si electrode (Fig. 1C), many spherical Si NPs and some irregular conductive carbon black NPs were observed, which agglomerated non-uniformly to form porous electrode structure. For the Si/G/PANI composite electrode (Fig. 1D), some misty films were present on the surfaces of Si, graphite and carbon black particles, which should be attributed to the amorphous polyaniline. It could be seen that the agglomeration of Si NPs was alleviated by the addition of polyaniline, suggesting that polyaniline facilitated the distribution of Si NPs. In addition, the image of

the Si/G/PANI composite showed better clearness than that of pure Si, where some white spots appeared (indicated by circles in Fig. 1C) because the low conductive Si tended to charge when scanned by electron beams. This result suggested that the conductive polyaniline improved electronic conductivity of the Si/G/PANI composite, which would lead to improved charge/discharge capacity.

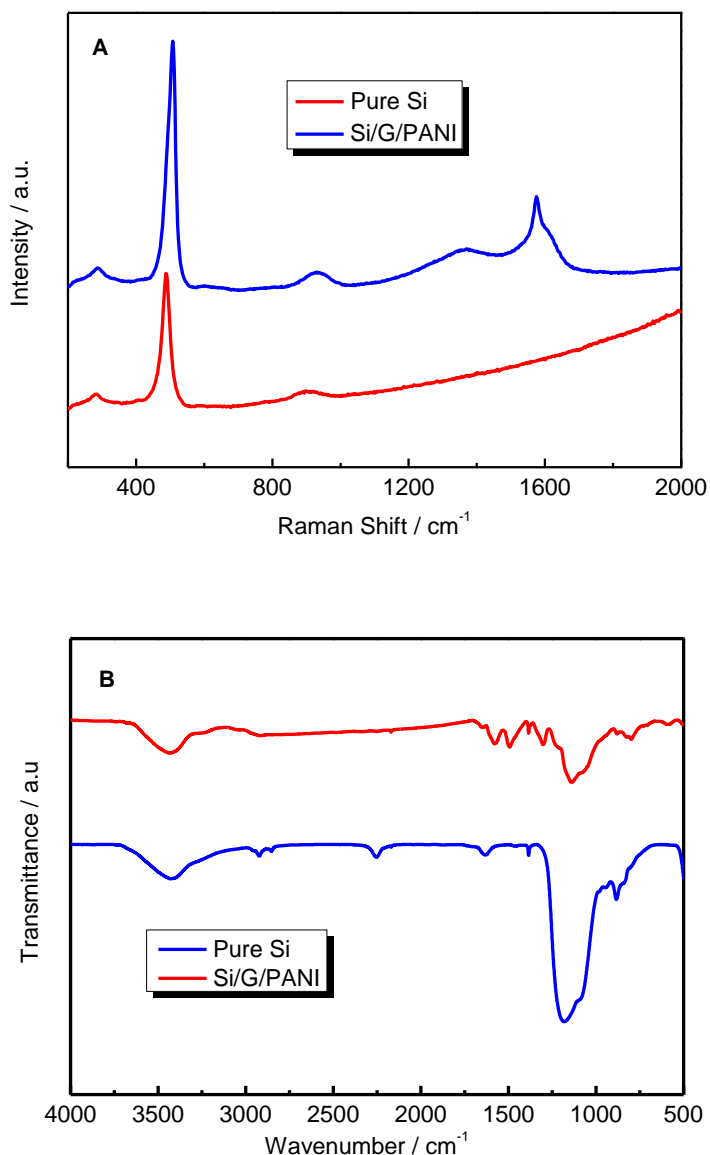


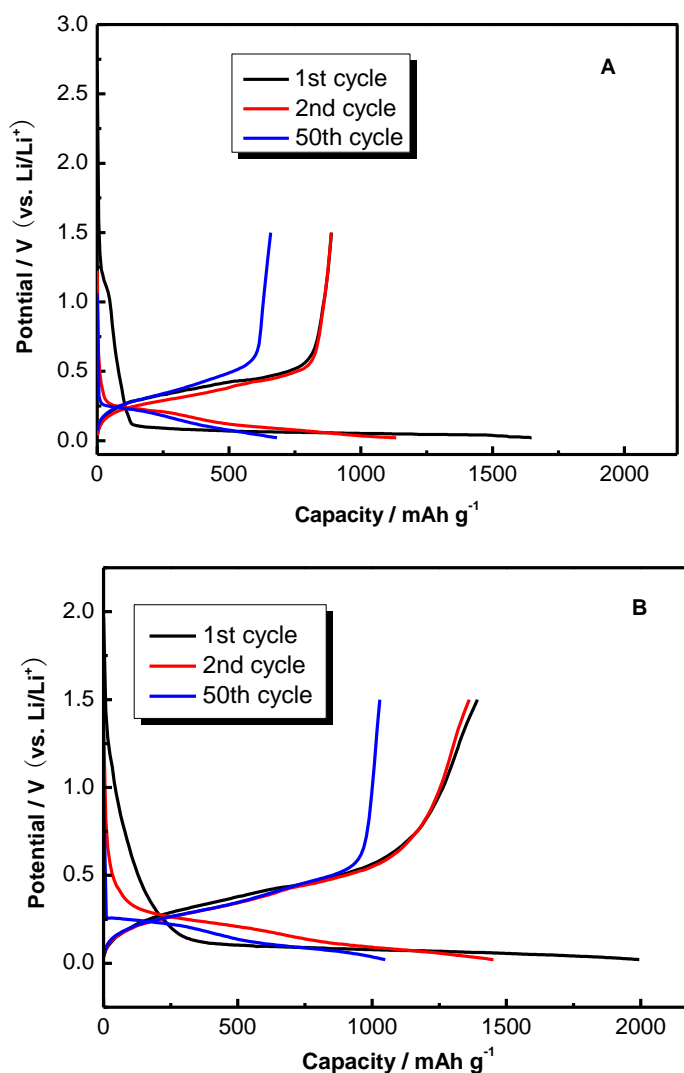
**Figure 2.** Raman (A) and FTIR (B) spectra for the Si/G/PANI composite and pure Si nanoparticles.

Raman and FTIR spectroscopy were carried out to verify that polyaniline had been successfully synthesized in the Si/G/PANI composite. A typical Raman spectrum for the Si/G/PANI composite is shown in Fig. 2A, where the Raman spectrum of pure Si is also plotted for comparison. For the Si/G/PANI composite, the peaks located at 1575 and 1367 cm<sup>-1</sup> corresponded to the C=C and C-C stretching in the quinoid rings, respectively [19]. Furthermore, compared to the pure Si, the Si/G/PANI composite showed a greatly enhanced peak at ~500 cm<sup>-1</sup>. This enhancement was due to the fact that the

characteristic C=N stretching band of polyaniline was superimposed on that assigned to Si [19, 20]. Fig. 2B presents the FTIR spectra for pure Si and the Si/G/PANI composite. For pure Si NPs, the characteristic peaks around 2800-3000  $\text{cm}^{-1}$  and 2254  $\text{cm}^{-1}$  were assigned to the C-H stretching vibrations of alkyl chains, which might originate from the remaining ethanol during the pretreatment of Si nanoparticles, and the Si-H stretching vibrations, respectively. For the Si/G/PANI composite, however, these peaks disappeared and three new peaks are observed at 1494, 1385 and 1304  $\text{cm}^{-1}$ , which belonged to the N-H deformation vibrating, the C=C stretching and the  $\text{CH}_2$  scissor vibrating, respectively [21]. These observations offered strong evidence for the presence of polyaniline in the Si/G/PANI composite, revealing that polyaniline was successfully synthesized.

### 3.2 Electrochemical performance

The galvanostatic charge-discharge profiles of the pure Si electrode are presented in Fig. 3A.



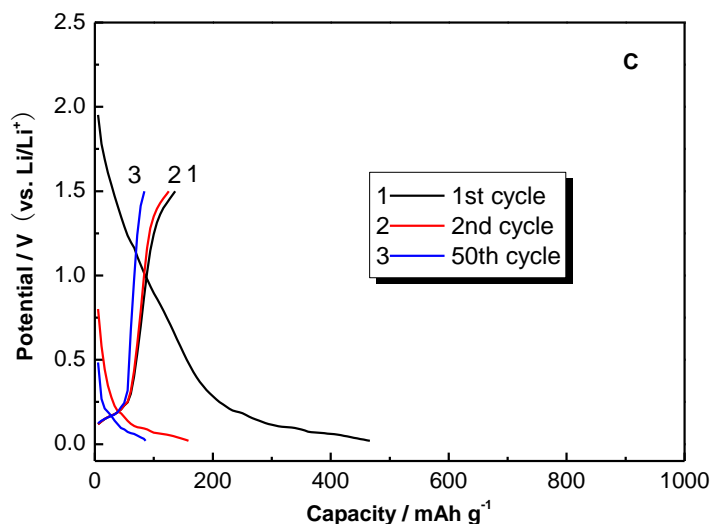


**Figure 3.** Galvanostatic charge-discharge curves for the pure Si (A), the Si/G/PANI composite (B) and the G/PANI composite (C).

During the first charge (Li intercalation), the potential decreased steadily to  $<0.15$  V at initial stage, which was reported to be associated with the formation of solid electrolyte interface (SEI) films and the reactions of Li with some oxides on Si and copper collector surfaces [22]. Then, the profile showed a broad and gently sloping plateau between 0.12 and 0.08 V, corresponding to the reaction of Li with Si to form the  $\text{Li}_x\text{Si}$  alloys [23].

During the first discharge (Li extraction), there is a single flat potential plateau, indicating the two-phase region of  $\text{Li}_x\text{Si}$  alloys, followed by an upwardly sloping region, suggesting the single-phase region of  $\text{Li}_x\text{Si}$  alloys with a small  $x$  value [23]. At the first cycle, the pure Si electrode delivered a discharge capacity of  $888 \text{ mAh g}^{-1}$  and had an irreversible capacity loss of  $759 \text{ mAh g}^{-1}$ , indicating a 53.9% of coulombic efficiency. Such a large irreversible capacity loss is common for Si electrodes and presumably arises from the electrolyte decomposition, the electrically disconnected particles due to the large volume changes, and the Li atoms “trapped” in the electrically connected particles [24]. On subsequent cycling, the charge profiles were different from the first charge, showing a sharply decreased potential followed by a more sloping plateau at about 0.2 V, whereas the discharge curves exhibited no appreciable changes from the first discharge. Apparently, after the first cycle, the charge/discharge capacities gradually approached to each other, indicating that the irreversible capacity loss was significantly reduced.

Fig. 3B shows the charge-discharge profiles for the Si/G/PANI composite electrode. It could be seen that these profiles were similar to those of pure Si (Fig. 3A), indicating that the presence of polyaniline did not block the Li intercalation/extraction process. On the contrary, both the discharge capacity and coulombic efficiency of the Si/G/PANI composite were greatly increased ( $1392 \text{ mAh g}^{-1}$  and 69.8 % for the first cycle), suggesting that polyaniline was highly effective in reinforcing the electronic contact and accommodating the severe volume change of Si nanoparticles. For comparison, galvanostatic charge-discharge behaviors of the G/PANI composite were also examined, and the results are shown in Fig. 3C. It was found that the reversible discharge capacity of the G/PANI

composite was  $<150 \text{ mAh g}^{-1}$ , so that the large reversible capacity of the Si/G/PANI composite resulted mainly from the active Si material.

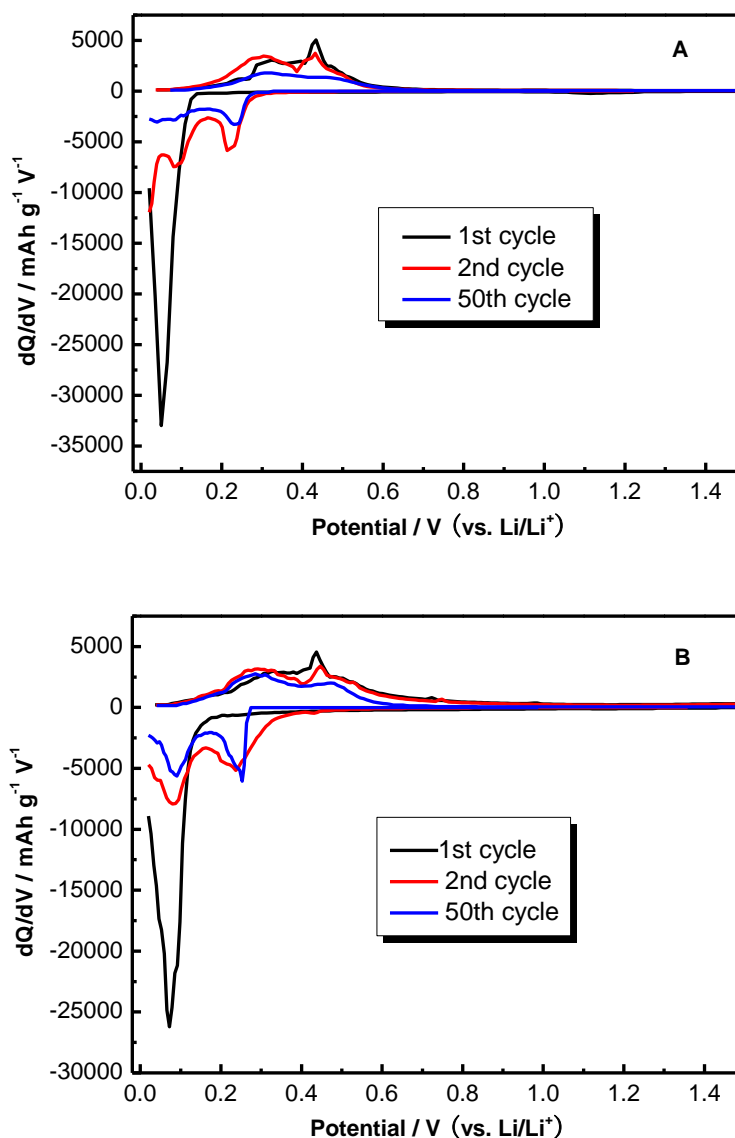


**Figure 4.** Differential capacity curves of the pure Si (A) and the Si/G/PANI composite (B) electrodes.

The differential capacity plots for the Si/G/PANI composite are shown in Fig. 4, where those of pure Si are also presented as a reference. The Si/G/PANI composite exhibited similar differential capacity profiles to pure Si. During the first charge, a large peak was observed at  $\sim 0.05 \text{ V}$ , which was associated with the two-phase region where crystalline Si reacted with Li to form amorphous  $\text{Li}_x\text{Si}$  alloys, corresponding to the long sloping plateau in Fig. 3B. Upon the first discharge, two peaks were present at  $\sim 0.31 \text{ V}$  and  $\sim 0.43 \text{ V}$ , respectively, indicative of different transformation processes between amorphous  $\text{Li}_x\text{Si}$  phases [25]. The following charge curves showed notably different feature: the emergence of two lithiation peaks at  $\sim 0.21 \text{ V}$  and  $\sim 0.09 \text{ V}$ , suggesting that crystalline Si changed into

amorphous states after only one cycle. It was noteworthy that, compared to pure Si, there were no apparent peaks corresponding to Li interaction with polyaniline, also indicating that polyaniline did not significantly contribute to the reversible capacity of the Si/G/PANI composite.

To further understand the improved electrochemical performance of the Si/G/PANI composite, EIS measurements were conducted after discharging the electrodes to 1.5 V, namely a 100% delithiation state. The EIS Nyquist plots for both Si/G/PANI composite and pure Si electrodes are presented in Fig. 5.

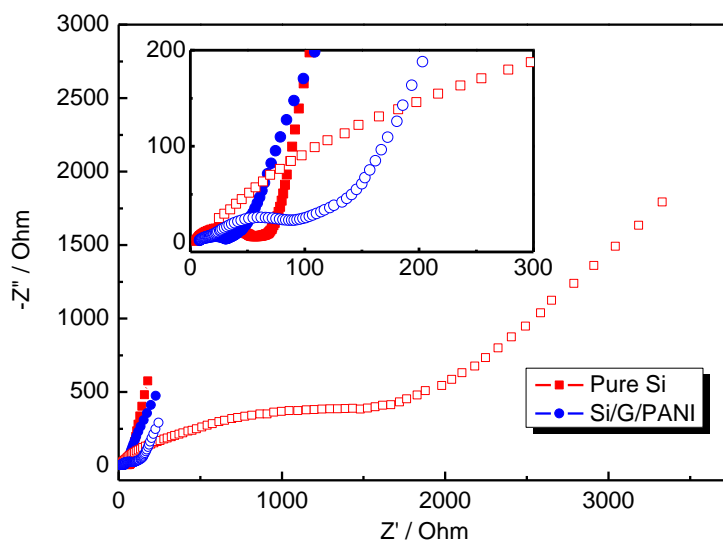


**Figure 5.** Nyquist plots of the Si/G/PANI composite and pure Si electrodes for the first (solid) and the 20<sup>th</sup> (hollow) cycles. Inset: magnified Nyquist plots.

These Nyquist plots consisted of one depressed semicircle in the high frequency (HF) region and a following around 45° quasi-line in the low frequency region. It has been reported that the diameter of the HF semicircle is closely associated with the interparticle contact resistance, apart from the charge-transfer process, after the electrode is fully discharged [26,27]. With the addition of polyaniline, the diameter of the semicircle for the Si/G/PANI composite was greatly reduced. Furthermore, after 20 cycles, the increase in the semicircle diameter for the Si/G/PANI composite was substantially lower than that for the pure Si. These results suggested that the interparticle contact resistance of the Si/G/PANI composite was significantly decreased, which was apparently due to the fact that polyaniline could alleviate the severe volume change of Si, and thus facilitated the contact of electrode materials, usually leading to improved reversible capacity.

The cycling life of the Si/G/PANI composite and pure Si was monitored and the results are given in Fig. 6. The discharge capacity of the Si/G/PANI composite was high (~1400 mAh g<sup>-1</sup>) and stable during the whole cycling test. After 95 cycles, the Si/G/PANI composite still delivered a discharge capacity of 866 mAh g<sup>-1</sup>, and the capacity retention was over 63%. In contrast, the cycling stability of pure Si was apparently inferior to that of the Si/G/PANI composite. After the same cycles, the discharge capacity of the pure Si electrode dropped to 425 mAh g<sup>-1</sup>, indicating the capacity

retention of 47%, as a result of the severe volume change during the Li intercalation/extraction processes. The reason for cycling improvement of the Si/G/PANI composite was clearly due to the fact that the Si/G/PANI composite could offer a good conductive and stress-alleviated environment to keep the stability of electrode configuration, and improve the cycling life.

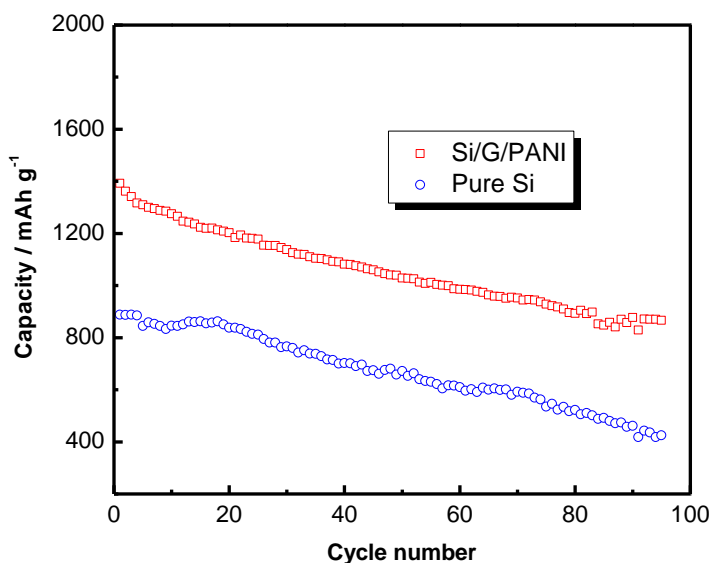


**Figure 6.** Cycling performance of the Si/G/PANI composite and the pure Si electrodes.

#### 4. CONCLUSIONS

We have reported a Si/G/PANI nanocomposite that can be facilely synthesized by the in-situ chemical polymerization of aniline monomer in the presence of Si nanoparticles and graphite. This composite consists of nanosized silicon and graphite embedded in a soft conductive polymer matrix, which offers the advantages of alleviating the severe volume changes, reinforcing the contact of electrode materials, and achieving better dispersion of Si nanoparticles. Thus, the composite shows a high reversible capacity of  $\sim 1392 \text{ mAh g}^{-1}$  with an improved initial coulombic efficiency of 69.8% and good cycleability with capacity retention of  $>63\%$  after 95 cycles, indicating that the Si/G/PANI composite is a promising LIB anode material. Also, the simplicity and effectiveness of this technique provide great flexibility and potential for the design and synthesis of other anode and cathode materials for LIBs.

#### ACKNOWLEDGEMENT

This work was financially supported by the Harbin Talents Foundation in the Innovation of Science and Technology under contact No. 2008RFQXG059, the Natural Scientific Research Innovation Foundation in Harbin Institute of Technology, and the National Science Foundation of China under contract No. 20706010 and 20876029.

## References

1. M. Endo, C. Kim, K. Nishimura, T. Fujino and K. Miyashita, *Carbon*, 38 (2000) 183.
2. S.B. Ng, J.Y. Lee and Z.L. Liu, *J. Power Sources*, 94 (2001) 63.
3. L. Wang, C.X. Ding, L.C. Zhang, H.W. Xu, D.W. Zhang, T. Cheng and C.H. Chen, *J. Power Sources*, 195 (2010) 5052.
4. Y. Yu, L. Gu, C.B. Zhu, S. Tsukimoto, P.A. van Aken and J. Maier, *Adv. Mater.*, 22 (2010) 1.
5. M. Yoshio, H. Wang, K. Fukuda, T. Umeno, N. Dimov and Z. Ogumi, *J. Electrochem. Soc.*, 149 (2002) A1598.
6. V.G. Khomenko and V.Z. Barsukov, *Electrochim. Acta*, 52 (2007) 2829.
7. C. Martin, M. Alias, F. Christien, O. Crosnier, D. Belanger and T. Brousse, *Adv. Mater.*, 21 (2009) 4735.
8. H. Kim, M. Seo, M.H. Park and J. Cho, *Angew Chem. Int. Ed.*, 49 (2010) 2146.
9. M. Uehara, J. Suzuki, K. Tamura, K. Sekine and T. Takamura, *J. Power Sources*, 146 (2005) 441.
10. Q. Si, K. Hanai, T. Ichikawa, A. Hirano, N. Imanishi, Y. Takeda and O. Yamamoto, *J. Power Sources*, 195 (2010) 1720.
11. P.J. Zuo, G.P. Yin, Z.L. Yang, Z.B. Wang, X.Q. Cheng, D.C. Jia and C.Y. Du, *Mater. Chem. Phys.*, 115 (2009) 757.
12. Z.S. Wen, J. Yang, B.F. Wang, K. Wang and Y. Liu, *Electrochem. Commun.*, 5 (2003) 165.
13. P. Gu, R. Cai, Y.K. Zhou and Z.P. Shao, *Electrochim. Acta*, 55 (2010) 3876.
14. Z. Luo, D.D. Fan, X.L. Liu, H.Y. Mao, C.F. Yao and Z.Y. Deng, *J. Power Sources*, 189 (2009) 16.
15. S.H. Ng, J.Z. Wang, D. Wexler, S.Y. Chew and H.K. Liu, *J. Phys. Chem. C*, 111 (2007) 11131.
16. A. Puda, N. Ogurtsova, A. Korzhenkova and G. Shapoval, *Prog. Polym. Sci.*, 28 (2003) 1701.
17. F.Y. Yang, Y. Chu, S.Y. Ma, Y.P. Zhang and J.L. Liu, *J. Colloid Interface Sci.*, 301 (2006) 470.
18. Z.P. Guo, J.Z. Wang, H.K. Liu and S.X. Dou, *J. Power Sources*, 146 (2005) 448.
19. J. Yang, X. Wang, X. Wang, R. Jia and J. Huang, *J. Phys. Chem. Solids*, 71 (2010) 448.
20. P. Unifantowicz, S. Vaucher, M. Lewandowska and K. Kurzydłowski, *J. Phys.: Condens. Matter*, 20 (2008) 025205.
21. B. Chen, A. Flatt, H. Jian, J. Hudson and J. Tour, *Chem. Mater.*, 17 (2005) 4832.
22. Y. Xu, G. Yin, Y. Ma, P. Zuo and X. Cheng, *J. Mater. Chem.*, 20 (2010) 3216.
23. M.N. Obrovac and L.J. Krause, *J. Electrochem. Soc.*, 154 (2007) A103.
24. J. Li and J. R. Dahn, *J. Electrochem. Soc.*, 154 (2007) A156.
25. C.K. Chan, R. Ruffo, S.S. Hong, R.A. Huggins and Y. Cui, *J. Power Sources*, 189 (2009) 34.
26. Y. Zhang, X.G. Zhang, H.L. Zhang, Z.G. Zhao, F. Li, C. Liu and H.M. Cheng, *Electrochim. Acta*, 51 (2006) 4994.
27. H.S. Kim, K.Y. Chung and B.W. Cho, *J. Power Sources*, 189 (2009) 108.